J. Non-Newtonian Fluid Mech. 165 (2010) 174–183

Contents lists available at ScienceDirect

Journal of Non-Newtonian Fluid Mechanics

journal homepage: www.elsevier.com/locate/jnnfm

# Study on the pulsating flow of a worm-like micellar solution

E. Emilio Herrera[a], F. Calderas[b,*], A.E. Chávez[a], O. Manero[b]

[a] Departamento de Ingeniería Química, Facultad de Química, Universidad Nacional Autónoma de México, México D.F., 04510, Mexico
[b] Departamento de Reología y Mecánica de Materiales, Instituto de Investigaciones en Materiales, Universidad Nacional Autónoma de México, México D.F., 04510, Mexico

ARTICLE INFO

*Article history:*
Received 3 July 2009
Received in revised form
14 September 2009
Accepted 18 November 2009

*Keywords:*
Complex liquids
Pulsatile flow
Stochastic solution
BMP model

ABSTRACT

In this work, the rectilinear flow of a complex liquid under a pulsating, time-dependent pressure gradient is analyzed. The fluctuating component of the pressure gradient is assumed to be of small amplitude and can be adequately represented by a weakly stochastic process, for which a quasi-static perturbation solution scheme is suggested. The pulsating pressure-gradient flow is analyzed with the Bautista–Manero–Puig model (BMP) constitutive equation, consisting in the upper convected Maxwell equation coupled to a kinetic equation to account for the breakdown and reformation of the fluid structure. According to the BMP model, thixotropy was found to have a negative effect on the energy associated to the maximum flow enhancement and reflects the relationship among the kinetic, viscous and structural mechanisms in the system. The flow enhancement is a function of the square of the amplitude of the oscillations, the Reynolds and Weissenberg numbers, and it is also dependent on the dimensionless numbers representing the viscoelastic, kinetic and structural mechanisms. Finally, flow enhancement is predicted in an aqueous worm-like micellar solution of cetyltrimethyl ammonium tosilate (CTAT) for various concentrations.



## 1. Introduction

The analysis of the oscillating pressure gradient flow of Newtonian and non-Newtonian fluids has attracted ample interest due to several applications, among them, in bio-fluid mechanics [1–3], biorheology, enhanced oil recovery and others. In biorheology, examples are the flow of blood in veins which is forced by a periodic pressure gradient [4–10] and interesting manifestations of biological fluid flow such as the flow of spider silk [11–13]. From a practical point of view, pulsatile flow of complex liquids (worm-like micellar systems and lyotropic liquid crystals) has applications in enhanced oil recovery. Likewise, pulsating and oscillating flows are important in the industrial applications such as polymer extrusion using oscillatory dies. The effect of the oscillations on the heat transfer and their interplay with inertia and viscous dissipation in non-Newtonian fluids, such as the dependency of the bulk temperature on frequency and amplitude of the oscillations, has been reported [14–21]. In addition, the use of pulsations has also been of interest in connection with heat, turbulent heat, mass transfer and coating processes [22–24].

Constitutive equations that take into account build-up and break-down kinetics of a complex fluid structure have been used to model several complex systems [25]. Complex fluids include biological fluids such as polypeptides, cellulose, and composites, that often exhibit crystalline order, anisotropy and viscoelasticity. They incorporate sequences of self-assembly, structural, kinetic processes under flow and mass transfer [26]. The characterization of these phenomena has been studied at length by several authors [27–31].

Likewise, viscoelastic surfactants have been used as rheological modifiers in coating process and also in enhanced oil recovery operations, especially those related to underground formations. The extraction of additional amounts of oil can be achieved by hydraulically inducting fractures in the rock formations [32]. Viscoelastic surfactants are characterized by entangled network of large worm-like micelle structures. These structures break and reform during flow, exhibiting a rich rheological behavior. Predictions of the flow behavior of viscoelastic surfactants by constitutive equations have been a challenging issue [33,34]. These systems exhibit Maxwell type behavior in small-amplitude oscillatory shear flow and saturation of the shear stress in steady simple shear, which leads to thixotropy and shear banding flow [35–37]. In the nonlinear viscoelastic regime, elongated micellar solutions also exhibit remarkable features, such as the presence of a stress plateau in steady shear flow past a critical shear rate accompanied by slow transients to reach steady state [38,39].

Theoretical predictions using perturbation and numerical methods on viscometric flows (or nearly viscometric flows) of the flow enhancement as a function of frequency and amplitude of oscillations have been reported [39–71], using viscous and viscoelastic

* Corresponding author. Tel.: +52 55 55585517; fax: +52 55 56224602.
*E-mail address:* almotasim@hotmail.com (F. Calderas).

0377-0257/$ – see front matter © 2009 Elsevier B.V. All rights reserved.
doi:10.1016/j.jnnfm.2009.11.001

equations of state [39–41,49,50,54,55,57–60,67–71]. In most analyses, it is shown that shear-thinning causes the flow enhancement and that this enhancement is proportional to the square of the relative amplitude of the oscillating pressure gradient and its magnitude depends strongly on the shape of the viscosity function. The maximum in the resonance curves reported by several authors can be explained by a coupling of the viscoelastic properties with the macroscopic perturbed motion. Among the important quantities are the shape of the viscosity curve and the inter-relation of the characteristic material properties of the system [54–60]. Other important factors are the wave-form (triangular, sinusoidal, and square type) that has a strong effect on flow enhancement and power requirements [64,65,68–70].

Notwithstanding, there is still open questions and lack of theoretical and experimental studies dealing with complex fluids and complex behaviors such as thixotropy, rheopexy and shear-banding in pulsating and oscillating flows. They represent a test to new constitutive equations and this aspect motivates the present investigation. In this regard, the main objectives of this work are:

1. Predictions of the flow enhancement and power requirement by a pulsating time pressure gradient of a complex kinetic liquid modelled by the Bautista–Manero–Puig (BMP) equation of state [72–75].
2. Analysis of the thixotropy and the inter-play with the kinetic, structural and viscoelastic properties of the fluid, through dimensionless groups associated to each mechanism.
3. Study the effect of the surfactant concentration on thixotropy using rheometric data of an aqueous worm-like micellar solution (cetyl trimethyl ammonium tosilate) to predict the flow enhancement for various micellar concentrations [76].

This paper is organized as follows: Section 1 contains the introduction to the problem and previous work. Section 2 discusses the BMP model. The formulation to the problem is presented in Section 3, with the non-dimensional variables and the stochastic properties of the random function $n(t)$ used to describe the pulsating pressure gradient. In Section 4, the perturbation solution is proposed and analytical results are shown in Section 5. Theoretical predictions of the flow enhancement using worm-like solutions data are described in Section 6. Concluding remarks and future work are mentioned in the last two sections.

## 2. Constitutive equation (the BMP model)

The BMP model [72–75] couples a time dependent equation for the structure changes with the upper-convected Maxwell constitutive equation. The evolution equation for the structural changes was conceived to account for the kinetic process of breakage and reformation of complex liquid and is defined by the following set of equations:

$$\underline{\underline{\sigma}} + \frac{\eta(II_{\underline{\underline{D}}})}{G_0}\overset{\nabla}{\underline{\underline{\sigma}}} = 2\eta(II_{\underline{\underline{D}}})\underline{\underline{D}} \tag{1}$$

$$\frac{d}{dt}\ln\ \eta(II_{\underline{\underline{D}}})^{\lambda} = 1 - \frac{\eta(II_{\underline{\underline{D}}})}{\eta_0} + k\lambda\left(1 - \frac{\eta(II_{\underline{\underline{D}}})}{\eta_\infty}\right)\underline{\underline{\sigma}} : \underline{\underline{D}} \tag{2}$$

In Eq. (1) the stress $\underline{\underline{\sigma}}$ is a viscoelastic stress, $\overset{\nabla}{\underline{\underline{\sigma}}}$ is the upper-convected derivative of the stress tensor, $\eta$ is the viscosity function, $\underline{\underline{D}}$ is the rate of deformation tensor, $II_{\underline{\underline{D}}}$ is the second invariant of $\underline{\underline{D}}$ and $G_0$ is the elastic modulus. In Eq. (2) $\eta_0$ and $\eta_\infty$ are the viscosities at zero and very high shear rates, respectively, $\lambda$ is the structural relaxation time and $k$ can be interpreted as a kinetic constant for the structure breakdown; all five parameters of the model ($\eta_0$, $\eta_\infty$, $G_0$, $\lambda$, and $k$) are related to the fluid properties and can be estimated from independent rheological experiments in steady and unsteady flows. The viscosity at lower and upper shear rates ($\eta_0$, $\eta_\infty$) can be estimated through experiments in steady shear flow. The structural time and elastic modulus ($G_0$, $\lambda$) can be calculated by using linear oscillatory flow. The parameter ($k$) can be evaluated in stress relaxation experiments after steady shear flow [76,77].

The BMP model was selected for this study due to its ability to predict the thixotropic behavior of structured fluids (such as worm-like micellar solutions, dispersions of lamellar liquid crystals, bentonite suspensions and associative polymers) [72–78]. It reproduces the flow curve of shear-thinning fluids, i.e. a Newtonian plateau at low and high shear rates and the intermediate power law region. Due to its simplicity, analytical solutions for complex flow situations can be explored, as compared to other more complex models [79–84].

## 3. Problem formulation

The isothermal rectilinear flow of an incompressible complex liquid under a pulsating time-dependent pressure gradient is analyzed in a circular pipe of radius $r = a$ and axial length $z = L$. Entry and exit effects and gravitational forces are neglected. In this system, all physical quantities in cylindrical coordinates $(r, \theta, z)$ are defined with respect to an origin at the pipe center. The axial fluid velocity is a function of $(r, t)$ and both the non-slip condition ($V_z(r = a, t) = 0$) and symmetry of the velocity field are applied. The pulsating pressure gradient here is represented by $\partial_z p(1 + \varepsilon n(t))$, where $n(t)$ is a pressure gradient noise and $\varepsilon \ll 1$ is a small parameter.

### 3.1. Dimensionless variables, groups and equations

#### 3.1.1. Non-dimensional variables

Herrera et al. [71,85] proposed the following dimensionless variables for the axial velocity, pressure gradient, time, shear-stress, shear-rate, radial coordinate, viscosity function and frequency, respectively

$$V_z^* = \frac{V_z}{\omega a};\quad p = \frac{dP/dz}{\eta_0/a\lambda};\quad t^* = \frac{t}{\lambda};\quad \tau = \frac{\sigma_{rz}}{\eta_0/\lambda};$$

$$N_{(1)}^* = \frac{N_1}{\eta_0/\lambda} = \frac{\sigma_{rr} - \sigma_{\theta\theta}}{\eta_0/\lambda}$$

$$N_{(2)}^* = \frac{N_2}{\eta_0/\lambda} = \frac{\sigma_{\theta\theta} - \sigma_{zz}}{\eta_0/\lambda};\quad \dot{\gamma}^* = \lambda\dot{\gamma}_{rz};$$

$$r^* = \frac{r}{a};\quad \eta^* = \frac{\eta}{\eta_0};\quad \omega^* = \omega\lambda \tag{3}$$

Here, the characteristic time is $\lambda$ (structural build-up time). This election of the non-dimensional variables enables the comparison with other characteristic times associated to a given physical mechanism (e.g. viscoelastic, $\lambda_0 = \eta_0 G_0^{-1}$, $\lambda_\infty = \eta_\infty G_0^{-1}$ and rupture $\lambda_r = k\eta_0$ times).

#### 3.1.2. Non-dimensional groups

Using the above expressions, the dimensionless components of the momentum equation, constitutive equations and the flow enhancement are obtained. In addition, the following non-dimensional groups are defined, as discussed previously by Herrera et al. [71,85]

$$Re = \frac{\rho(\omega a)a}{\eta_0};\quad De = \frac{\eta_0 G_0^{-1}}{\lambda};\quad A = \frac{k\eta_0}{\lambda};\quad B = \frac{\eta_0}{\eta_\infty};$$

$$C = (AB)^{1/2} = \left(\frac{k\eta_0}{\lambda}\frac{\eta_0}{\eta_\infty}\right)^{1/2};\quad We = \omega^* De = \frac{\eta_0}{G_0}\omega;$$

$$ReWe = \frac{\rho(\omega a)^2}{G_0} \tag{4}$$

The pulsating Reynolds number (Re) [53] relates the inertial and viscous forces in the fluid. The second group is the Deborah number ($De$), which represents the relation between two characteristic times, the Maxwell relaxation time (which is associated to the viscoelastic properties of the fluid $\lambda_0 = \eta_0 G_0^{-1}$) and the structure relaxation time (which is a structure buildup time $\lambda$). The third non-dimensional number ($A$) is a relationship between the kinetic and viscous processes for structure breakdown (destruction function) and the structural recovery time $\lambda$. The fourth group ($B$) is the ratio of the viscosities at low and high shear rates. This group is a measure of the shear-thinning ($B>1$) and shear-thickening ($B<1$) behavior. Finally the last group is a product of the dimensionless numbers $A$ and $B$. This group can be interpreted as the square ratio of two geometrical mean relaxation times (defined as $\lambda_r = k\eta_0$, $\lambda_0 = \eta_0 G_0^{-1}$, $\lambda_\infty = \eta_\infty G_0^{-1}$), so the dimensionless number $C$ can be rewritten as $C = \sqrt{AB} = \lambda_G^I/\lambda_G^{II} = \sqrt{\lambda_r\lambda_0}/\sqrt{\lambda\lambda_\infty} = \sqrt{\lambda_r(\lambda_0/\lambda\lambda_\infty)}$. The time $\lambda_G^I$ is associated to the structure rupture and Maxwell time and $\lambda_G^{II}$ is related to the structural and high shear-rate characteristic times. As particular cases, when $\lambda_r = k\eta_0 = \lambda\lambda_0\lambda_\infty^{-1}$, $C$ reduces to the dimensional $B$, i.e. $C=B$, which is a measure of the shear-thinning ($B>1$) or shear-thickening ($B<1$) properties of the system. Similarly, when $\lambda_r = k\eta_0 = \lambda_\infty\lambda_0\lambda^{-1}$, $C=De$ is obtained. It is important to note that if $C>1$, the rupture and viscoelastic relaxation times dominate over the structural and characteristic time at high shear rates. In contrast, if $C<1$, the effects of the structural and high shear-rate times are the dominant mechanisms. Moreover, the effects of the thixotropy are included as a particular case of the kinetics, viscous and structural mechanism when the kinetic constant is identified as normalized constant for shear stress, i.e. $k = G_0^{-1}$. In general the non-dimensional number satisfies the inequality: $De \supset A \le C \le B$. The next group is the pulsating Weissenberg number, which is a product between Deborah number and non-dimensional frequency $\omega^*$. As $We = \eta_0 G_0^{-1}\omega \to 0$, the BMP model reduces to the inelastic case. In contrast, as $We = \eta_0 G_0^{-1}\omega \to \infty$, the elastic effects are dominant. The last group is the product of the Reynolds and Weissenberg numbers. If $ReWe \gg 1$, inertial effects dominate over elastic properties. In contrast, if $ReWe \ll 1$, the opposite effect is manifested.

#### 3.1.3. Non-dimensional momentum equation

$$Re\frac{\partial V_z^*}{\partial t^*} = -p(1+\varepsilon n(t^*)) + \frac{1}{r^*}\frac{\partial}{\partial r^*}(r^*\tau) \tag{5}$$

and non-dimensional boundary conditions

$$V_z^*(r^*=1,t^*)=0 \quad \text{And} \quad \dot\gamma^*(0,t^*) = \frac{\partial}{\partial r^*}V_z^*(r^*,t^*)|_{r^*=0} = 0 \tag{6}$$

Notice that in Eq. (5), $n(t^*)$ is a stochastic dimensionless function.

#### 3.1.4. Non-dimensional BMP equation

The relevant components of the BMP model are:

$$\left(1 + De\ \eta^*(\dot\gamma^*)\frac{\partial}{\partial t^*}\right)\tau - De\,\eta^*(\dot\gamma^*)N_{(2)}^* = \eta^*(\dot\gamma^*)\dot\gamma^* \tag{7}$$

$$\frac{d}{dt^*}\ln\eta^*(\dot\gamma^*) = 1 - \eta^*(\dot\gamma^*) + A(1 - B\eta^*(\dot\gamma^*))\tau\dot\gamma^* \tag{8}$$

In the rest of the paper, the evolution equations of the first and second normal stress differences are not considered since they are not relevant for the calculation of the flow enhancement.

#### 3.1.5. Non-dimensional flow enhancement

$$I(\%) = 100\frac{\int_0^1(\langle\dot\gamma^*\rangle - \dot\gamma_0^*)r^{*2}\,dr^*}{\int_0^1\dot\gamma_0^* r^{*2}\,dr^*},\quad \langle\dot\gamma^*\rangle = \frac{\int_0^{2\pi/\omega^*}\dot\gamma^* dt^*}{\int_0^{2\pi/\omega^*}dt^*} \tag{9}$$

Experimentally, the Reynolds number given in Eq. (4) is sufficiently small [40,41,48,53–57,59,60] hence this term in Eq. (5) is neglected, i.e. $Re\,\partial V_z^*/\partial t^* \sim 0$. Similarly, experiments in micellar solutions, such as CTAT and EHAC [72–76], showed that the contribution of the second stress difference is small, so the third term in Eq. (7) can be neglected, i.e. $De\,\eta^*(\dot\gamma^*)N_{(2)}^* \cong 0$.

#### 3.1.6. Stochastic non-dimensional function

Analytical progress is possible if $n(t^*)$ is considered as a stationary random function of time, with correlation function $R(s)$ [86]

$$n(t^*) = \int_{-\infty}^{+\infty} e^{i\alpha t^*}\,dZ(\alpha) \quad R(s) = \left\langle\overline{n(t^*)}n(t^*+s)\right\rangle$$
$$= \int_{-\infty}^{+\infty} e^{i\alpha s}\Omega(\alpha)d\alpha \tag{10}$$

where $dZ(\alpha)$ is an interval random function of $\alpha$ with zero mean and uncorrelated increments

$$\langle dZ(\alpha)\rangle = 0 \quad \langle dZ(\alpha_i)d\bar Z(\alpha_j)\rangle = \delta_{ij}\Omega(\alpha_i)d\alpha_j$$

$$\Omega(\alpha) = \frac{1}{2\pi}\int_{-\infty}^{+\infty} e^{-i\alpha s}R(s)ds \tag{11}$$

In (10) and (11), $\langle\ \rangle$ denotes an ensemble average and the overbar a complex conjugate quantity, $\delta_{ij}$ is the Kronecker delta and $\Omega(\alpha)$ is the spectral density of $n(t^*)$. In Eqs. (10) and (11) it is assumed that $|R(s)|$ tends to zero fast enough as $|s|$ tends to infinity, a condition met by most, if not all physically realizable processes [54,55,57–60,71].

## 4. Perturbation scheme

Analytical expressions for the flow enhancement and power requirement require a quasi-static perturbation solution in terms of the small parameter $\varepsilon$ [40,47–52,54–57,59,60,71]. The shear-rate, viscosity and shear stress can be expressed in power series of $\varepsilon$ (provided $\varepsilon \ll 1$):

$$\begin{aligned}
\dot\gamma^*(r^*,t^*) &= \dot\gamma_0^*(r^*)\varepsilon^0 + \dot\gamma_1^*(r^*,t^*)\varepsilon^1 + \dot\gamma_2^*(r^*,t^*)\varepsilon^2 + \cdots\\
\eta^*(r^*,t^*) &= \eta_0^*(r^*)\varepsilon^0 + (\dot\gamma_1^*\dot\eta_0^*)\varepsilon^1 + \left(\dot\gamma_2^*\dot\eta_0^* + \frac{1}{2}\dot\gamma_1^*\ddot\eta_0^*\right)\varepsilon^2 + \cdots\\
\tau(r^*,t^*) &= \tau_0(r^*)\varepsilon^0 + (\dot\gamma_1^*\dot\tau_0)\varepsilon^1\left(\dot\gamma_2^*\dot\tau_0 + \frac{1}{2}\dot\gamma_1^{*2}\ddot\tau_0\right)\varepsilon^2 + \cdots
\end{aligned} \tag{12}$$

In (12), the Taylor theorem allows expressing $\tau_j(r^*,t^*)$ and $\eta_j^*(r^*,t^*)$ ($j\in I=\{0,1,2,\ldots\}$) in terms of the derivatives of $\tau_0(r^*)$ and $\eta_0^*(r^*)$, where the following shorthand notation has been used [54,55,57,60,71]

$$\dot\tau_0 = \left.\frac{d\tau(\dot\gamma^*)}{d\dot\gamma^*}\right|_{\dot\gamma^*\to\dot\gamma_0^*};\quad \ddot\tau_0 = \left.\frac{d^2\tau(\dot\gamma^*)}{d\dot\gamma^{*2}}\right|_{\dot\gamma^*\to\dot\gamma_0^*};$$

$$\dot\eta_0^* = \left.\frac{d\eta^*}{d\dot\gamma^*}\right|_{\dot\gamma^*\to\dot\gamma_0^*};\quad \ddot\eta_0^* = \left.\frac{d^2\eta^*}{d\dot\gamma^{*2}}\right|_{\dot\gamma^*\to\dot\gamma_0^*} \tag{13}$$

It is important to note that the particular perturbation expansions for the viscosity and the shear stress are different from other variable expansions, because it allows for the decoupling of the upper-convected Maxwell model from the kinetic equation of the BMP model. In addition, the flow enhancement can be expressed in terms of the higher derivatives of the shear stress and viscosity functions to zeroth order [54,55,57,60,71].

## 5. Asymptotic analyses

### 5.1. Zeroth-order theory

Substitution of Eqs. (12) and (13) into (5)–(9) and equating terms of the same order in the $\varepsilon$ parameter, leads to the zeroth solution, i.e. $O(\varepsilon^0)$:

$$\tau_0 = \eta_0^*\dot{\gamma}_0^* = \frac{A\dot{\gamma}_0^{*2} - 1 + \sqrt{\left(A\dot{\gamma}_0^{*2} - 1\right)^2 + 4AB\dot{\gamma}_0^{*2}}}{2AB\dot{\gamma}_0^{*2}}\dot{\gamma}_0^* = \tau_w r^* \tag{14}$$

In Eq. (14), $\tau_w = \tau_0(r^* = 1)$ is the wall stress and the boundary condition $\tau_0 = 0$ at $r^* = 0$ has been used. The first and second normal stress differences were calculated by Herrera et al. [71] ($N^*_{(1)0} = 2De\tau_0^2$, $N^*_{(2)0} = 0$). According to (9), no flow enhancement to zeroth-order is predicted, i.e. $I(\%) = 0$.

### 5.2. First-order theory

To first order in $\varepsilon$, i.e. $O(\varepsilon^1)$:

$$\tau_1(r^*, t^*) = \tau_0 n(t^*) \tag{15}$$

$$\dot{\gamma}_1^*(r^*, t^*) = \frac{\tau_0}{\dot{\gamma}_0}\left(n(t^*) + De\ \eta_0^*\dot{n}(t^*)\right); \quad \dot{\tau}_0 \neq 0 \tag{16}$$

$$I\ (\%) = 100\varepsilon\frac{\int_0^1 \langle\dot{\gamma}_1^*(r^*, t^*)\rangle r^{*2}\,dr^*}{\int_0^1 \dot{\gamma}_0^*(r^*)r^{*2}\,dr^*} \tag{17}$$

In Eqs. (15) and (16) the boundary conditions $\tau_1(r^*, t^*) = \dot{\gamma}_1^*(r^*, t^*) = 0$ at $r^* = 0$ were used. On the other hand, the average of Eq. (16) is zero, i.e. $\langle\dot{\gamma}_1^*(r^*, t^*)\rangle = 0$. As a consequence, the flow enhancement (Eq. (17)) to first order is again zero.

### 5.3. Second-order theory

To second order in $\varepsilon$, i.e. $O(\varepsilon^2)$ the shear stress is zero, i.e. $\tau_2(r^*, t^*) = 0$ and the shear strain and flow enhancement are given by the following equations:

$$\dot{\gamma}_2^*(r^*, t^*) = -\frac{1}{2}\frac{\ddot{\tau}_0}{\dot{\tau}_0}\dot{\gamma}_1^{*2}(r^*, t^*) + De\ \dot{\eta}_0^*\frac{\tau_0}{\dot{\tau}_0}\dot{n}(t^*)\dot{\gamma}_1^*(r^*, t^*); \quad \dot{\tau}_0 \neq 0 \tag{18}$$

$$\frac{I\ (\%)}{\varepsilon^2} = 100\frac{\int_0^1 \langle\dot{\gamma}_2^*(r^*, t^*)\rangle r^{*2}\,dr^*}{\int_0^1 \dot{\gamma}_0^*(r^*)r^{*2}\,dr^*} \tag{19}$$

In Eq. (18) the boundary condition $\dot{\gamma}_2^*(r^*, t^*) = 0$ at $r^* = 0$ was used. To calculate the flow enhancement, the average value of Eq. (18) is taken. Substitution of Eq. (16) into Eq. (18) and using the random stochastic definitions (10) and (11), the average shear rate to second order is obtained:

$$\langle\dot{\gamma}_2^*(r^*, t^*)\rangle = \frac{1}{2}\tau_0^2\left\{\frac{\ddot{\tau}_0}{\dot{\tau}_0^3}(R_0(0) + De^2\eta_0^{*2}R_1(0)) + De^2\frac{\dot{\eta}_0^{*2}}{\dot{\tau}_0^2}R_0(0)\right\} \tag{20}$$

where

$$R_0(0) = \int_{-\infty}^{+\infty}\Omega(\alpha)d\alpha; \quad R_1(0) = \int_{-\infty}^{+\infty}\alpha^2\Omega(\alpha)d\alpha \tag{21}$$

### 5.4. Particular stochastic random functions

#### 5.4.1. Harmonic random function (sinusoidal pressure wave form)

The simplest harmonic random function is given by a sinusoidal function with frequency $\omega^* = \lambda\omega$ and amplitude $M$ and its respectively spectral density $\Omega(\alpha)$, i.e.

$$n(t^*) = M\ \sin(\omega^* t^*) \quad \Omega(\alpha) = \frac{1}{4}(\delta(\alpha - \omega^*) + \delta(\alpha + \omega^*)) \tag{22}$$

the corresponding correlation functions $R_0(0)$ and $R_1(0)$ are given by:

$$R_1(0) = \omega^{*2}R_0(0) \quad \text{and} \quad R_0(0) = \langle n(t^*)n(t^* + 0)\rangle = \frac{1}{2}M^2 \tag{23}$$

The simplest election of a sinusoidal pressure wave enables the comparison with representative theoretical works [40,41,47,49–52,54–60,71]. Notice that the particular harmonic random function used here can be obtained in the limiting case of a Fourier-time series [64,65]. Phan-Thien [54] showed that the non-harmonic effects can increase or decrease the flow enhancement depending on the particular random function $n(t^*)$.

Next, Eq. (23) is substituted into Eq. (20), and then in Eq. (19) to give

$$\frac{I(\%)}{\varepsilon^2} = 25M^2\frac{\int_0^{\dot{\gamma}_w^*}\tau_0^4(-\ddot{\tau}_0/\dot{\tau}_0^2(1 + \omega^{*2}De^2\eta_0^{*2}) + \omega^{*2}De^2\,\dot{\eta}_0^{*2}/\dot{\tau}_0)d\dot{\gamma}_0^*}{\int_0^{\dot{\gamma}_w^*}\dot{\gamma}_0^* d(1/3\,\tau_0^3)} \tag{24}$$

It is important to note that when elastic effects dominate, the flow enhancement is negative and this can be attributed to the mathematical properties of the constitutive curve. Constitutive equations that contain a variable relaxation time depending on the second invariant of the rate of deformation tensor, i.e. $t_{rel} = \eta(II_D)G_0^{-1}$, such as (i) White–Metzner. BMP and modify BMP models, may predict negative flow enhancement [47,72,75]. Experimentally, the negative flow enhancement can be attributed to a flow transition. For example, in complex liquids (liquid crystals) the viscosity depends on position and oscillating orientation. This gives rise to flow enhancement under shear-thinning conditions and flow reduction under shear-thickening and backflow (or flow-induced re-orientation) [27–31,68–70].

Notwithstanding, experiments are necessary to validate the predictions of negative flow enhancement in complex liquids such as worm-like micellar solutions, dispersions of lamellar liquid crystals, bentonite suspensions or associative polymers [72–78].

Integrating by parts (24), the following expression for the flow enhancement is obtained

$$\frac{I(\%)}{\varepsilon^2} = 75M^2\frac{\tau_w^4 - 4\dot{\tau}_w\int_0^{\dot{\gamma}_w^*}\tau_0^3 d\dot{\gamma}_0^* + We^2\left(\tau_w^4\eta_w^{*2} - 4\dot{\tau}_w\int_0^{\dot{\gamma}_w^*}\eta_0^{*2}\tau_0^3 d\dot{\gamma}_0^*\right)}{\dot{\tau}_w\left(\dot{\gamma}_w^*\tau_w^4 - \int_0^{\dot{\gamma}_w^*}\tau_0^3 d\dot{\gamma}_0^*\right)} \tag{25}$$

In Eq. (25) $\eta_w^* = \eta_0^*(\dot{\gamma}_w^*)$, $\tau_w = \tau_0(\dot{\gamma}_w^*)$ are the viscosity function and stress at the wall, respectively. Bird et al. [47] used the White–Metzner model with an alternative perturbation technique and obtained a similar expression. Phan-Thien [50,54,55] obtained similar results for four different constitutive equations.

To solve the integrals given in (25), the following relationship between the wall shear-stress and the wall shear-rate in Eq. (14) is used:

$$\dot{\gamma}_w^*(\tau_w) = \frac{AB\tau_w^2 - 1 + \sqrt{(AB\tau_w^2 - 1)^2 + 4A\tau_w^2}}{2A\tau_w} \tag{26}$$

### 5.5. Time average power

The non-dimensional time-average power $\langle P\rangle = \langle Q\nabla_z p(1+\varepsilon n(t^*))\rangle$ (where $Q$ is the volumetric flow, $\nabla_z p(1+\varepsilon n(t^*))$ is the axial component of the pulsating pressure gradient) required to pump the fluid and the fractional increase in power $I_{pot}(\%)$ are given by $I_{pot}(\%)=100(\langle P\rangle - P_0/P_0)$, where $P_0$ is the non-dimensional power required to pump the fluid without pulsatile pressure and $\langle P\rangle$ is the average power with pulsatile flow. Upon substitution of the series given in (12) into $I_{pot}(\%) = 100(\langle P\rangle - P_0)P_0^{-1}$ and proceeding as before (Eqs. (14)–(25)), the power requirement is obtained:

$$\frac{I_{pot}(\%)}{\varepsilon^2} = 75M^2 \frac{\begin{array}{c}\tau_w^4 - 2\dot{\tau}_w \int_0^{\dot{\gamma}_w^*} \tau_0^3 d\dot{\gamma}_0^* \\ +We^2\left(\tau_w^4\eta_w^{*2} - 4\dot{\tau}_w\int_0^{\dot{\gamma}_w^*}\eta_0^{*2}\tau_0^3 d\dot{\gamma}_0^*\right)\end{array}}{\dot{\tau}_w\left(\dot{\gamma}_w^*\tau_w^3 - \int_0^{\dot{\gamma}_w^*}\tau_0^3 d\dot{\gamma}_0^*\right)} \tag{27}$$

The power requirement by the BMP model (Eq. (27)) has two contributions: inelastic and elastic and contain particular cases described in the literature (Tanner and Generalized Newtonian) [49,50,54]. Elasticity does not represent an advantage to pumping because the extra power required for the pulsating flow is always positive. This conclusion agrees with several previous works which used different constitutive equations [45,60].

### 5.6. Flow enhancement of the BMP as a function of dimensionless frequency

In the particular case where the pulsating Reynolds number is of the order of the small parameter $\varepsilon$, i.e. $\mathrm{Re} = O(\varepsilon)$ [47,49,50,51,54–60,71] the flow enhancement is dependent on the dimensionless frequency, according to Eq. (25), which may be cast in the following form:

$$I(\%) = 75M^2\beta^2\{\delta_1 + \delta_2\omega^{*2}De^2\}\omega^{*2} \tag{28}$$

and $\delta_1$, $\delta_2$ are given by:

$$\delta_1(A,B) = \frac{\tau_w^4 - 4\tau_w^*\int_0^{\dot{\gamma}_w^*}\tau_0^3 d\dot{\gamma}_0^*}{\dot{\tau}_w\left(\dot{\gamma}_w^*\tau_w^3 - \int_0^{\dot{\gamma}_w^*}\tau_0^3 d\dot{\gamma}_0^*\right)};$$

$$\delta_2(A,B) = \frac{\tau_w^2\eta_w^{*2} - 4\dot{\tau}_w\int_0^{\dot{\gamma}_w^*}\eta_0^{*2}\tau_0^3 d\dot{\gamma}_0^*}{\dot{\tau}_w\left(\dot{\gamma}_w^*\tau_w^3 - \int_0^{\dot{\gamma}_w^*}\tau_0^3 d\dot{\gamma}_0^*\right)} \tag{29}$$

where $\beta = (a^2/\lambda)/(\eta_0/\rho)$. Eq. (29) describes the flow enhancement as a function of the non-dimensional frequency when $\delta_1$ and $\delta_2$ are fixed. It is important to note that $\beta$ can be interpreted as a ratio between two diffusion coefficients. Proceeding as Herrera et al. [71], it is possible to obtain an analytical solution for the maximum flow as a function of the kinetic, structural, viscoelastic and inertial contributions through the non-dimensional numbers $(A, B, De, \beta)$ and the square of the amplitude of the oscillations.

$$I_{Max}(\%) = 2.34M^2\frac{\delta_1^2}{(-\delta_2)}\left(\frac{\beta}{De}\right)^2; \quad (-\alpha) > 0 \tag{30}$$

Eq. (30) is valid only in the limit of sufficiently low pulsating Reynolds number ($\mathrm{Re} \ll 1$) and satisfies the inequality: $0 \leq \beta\omega^* \ll 1 \Rightarrow 0 \leq \omega^* \ll \omega_C^* = \beta^{-1}$; consequently, the critical non-dimensional frequency ($\omega_C^* = \beta^{-1}$) is determined according to the ratio between structural and momentum diffusivities.

#### 5.6.1. Inelastic and elastic effects

Eq. (28) contains an asymptotic case for negligible small elastic and high effects, i.e. $\delta_1 \gg \omega^{*2}De^2\delta_2$ and $\delta_1 \ll \omega^{*2}De^2\delta_2$

$$\frac{I_1(\%)}{I_0(\%)} \cong \left(\frac{\omega_1^*}{\omega_0^*}\right)^2 \quad \text{and} \quad \frac{I_1(\%)}{I_0(\%)} \cong \left(\frac{\omega_1^*}{\omega_0^*}\right)^4 \tag{31}$$

$I_0$ (%) and $I_1$ (%) are the flow enhancements for dimensional frequencies $\omega_0^*$ and $\omega_1^*$, respectively. If $\omega_1^* = N\omega_0^*$; $(N \in R^+)$ equations given in (31) take the form:

$$I_1(\%) \cong (N)^2 I_0(\%) \quad \text{and} \quad I_1(\%) \cong (N)^4 I_0(\%) \tag{32}$$

## 6. Results

### 6.1. BMP theoretical predictions

The flow enhancement integral equation (25) was solved numerically by using a quadrature Gaussian method combined with a Lagrange method to extrapolate to zero mesh size. Without loss of generality, in all calculations the amplitude of the oscillations is set to one ($M = 1$). Predictions of the flow curve under steady shear flow have been reported elsewhere, Herrera et al. [71]. First and second Newtonian plateaus are predicted as well as an intermediate shear-thinning region. It is important to note that the shear stress function is a monotonically increasing function of the shear-rate and its derivative $\dot{\tau}_0 \neq 0$ is always positive. Nevertheless, the second derivative changes sign due to the convexity and concavity of the shear stress function.

In Fig. 1, the first and second derivatives of the flow curve are plotted. The parameters used in the simulation are $A = 1$ and $B = 1000$. At low shear-rates $10^{-3} \leq \dot{\gamma}_0^*(r^*) < 10^{-2}$ the first derivative of the shear-stress is almost constant. For moderate values of $\dot{\gamma}_0^*(r^*)(10^{-1} \leq \dot{\gamma}_0^*(r^*) < 2)$ it decreases monotonically. For $\dot{\gamma}_0^*(r^*) > 2$ the first derivative increases again and the flow enhancement decreases. Notice that the minimum corresponds to the shear-thinning region, where the system undergoes drastic structural changes. In contrast, the second derivative of the shear stress increases rapidly and reaches a maximum for moderate shear-rates, and for a critical shear-rate, it decreases monotonically to zero. Physically, the structure of the fluid undergoes a transition from an isotropic structure into an ordered-anisotropic structure under flow (first plateau and shear-thinning regions).

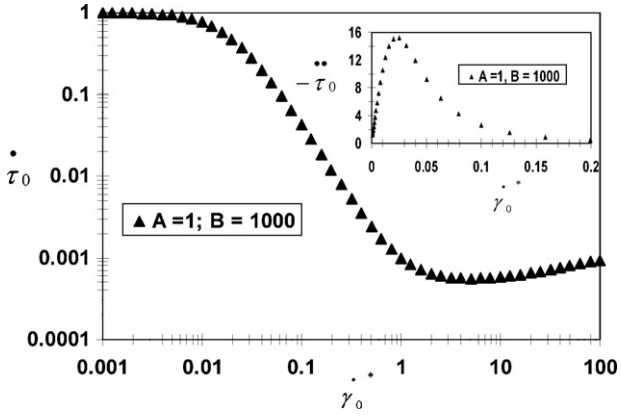


**Fig. 1.** First derivative of the shear-stress versus shear rate. Inset: second derivative of the shear-stress versus shear-rate. Non-dimensional numbers used in the simulation are: $A = 1$, $B = 1000$.

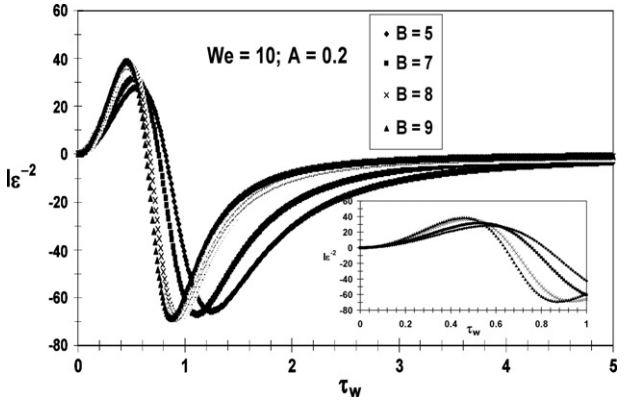


**Fig. 2.** Flow enhancement versus dimensionless wall stress for various values of $B$: (i) 1000, (ii) 1500, (iii) 2000, and (iv) 2500. The dimensionless groups employed in the simulation are: $We = 10$ and $A = 0.2$.

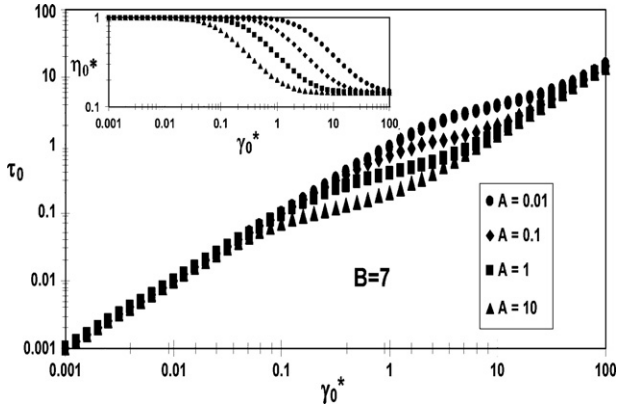


**Fig. 4.** Dimensionless shear stress versus shear-rate for $B = 7$ and various values of $A$: (i) 0.01, (ii) 0.1, (iii) 1, and (iv) 10. Inset: viscosity versus shear rate.

The wall shear-rate versus wall stress for various values of the non-dimensional number $B$ (representing various CTAT concentrations) follows the same tendency predicted previously by Herrera et al. [71] and for this reason is not shown. At low wall stresses an almost constant value is predicted and past a critical wall stress, the wall shear rate increases rapidly. For high wall stresses, the behavior of the wall shear-rate is constant throughout. Moreover, the asymptotic value increases as the fluid becomes more shear-thinning.

In Fig. 2, the flow enhancement $I\varepsilon^{-2}$ for a viscoelastic liquid versus the wall stress for various non-dimensional numbers $B$ is shown ($We = 10$, $A = 0.2$). Resonance behavior consisting in a maximum in the flow enhancement is observed at a critical wall stress, and the magnitude of this maximum increases as the shear-thinning character of the fluid becomes more predominant. A large minimum in the curves is also observed; the absolute magnitude of the minima depends on the shear thinning characteristics of the liquid. For large wall stresses, all curves asymptote to zero flow enhancement. Inset in Fig. 2 shows a zoom in the $x$-axis to highlight the shifting of the curves to low stresses and the increase in the maxima as $B$ increases. Up to the maximum of the curve, the flow enhancement is a monotonically increasing function of the wall stress and the magnitude of the maximum is entirely determined by a coupling between the structural and kinetics processes. After reaching the maximum, the flow enhancement decays to zero very fast.

In Fig. 3, the flow enhancement ($I\varepsilon^{-2}$) versus wall stress for various pulsating Weissenberg numbers is plotted. The parameters used in the simulation are $A = 0.2$ and $B = 7$. The line with triangle symbols shows the inelastic case where for any value of the shear-stress the flow enhancement is always positive, and tends to zero for $\tau_w > 1$. Nevertheless, when the elasticity is present, namely, $We > 0$, the maximum in the curves increases with $We$, and shifts to lower wall stresses as $We$ increases. A crossover point at a critical shear-stress is observed after which the flow enhancement becomes negative, and the minima of this reduction becomes more predominant as $We$ increases. However, in the experimental results for polymer solutions only positive values are observed. For example, several research works reported only positive values, with $I$ (%) sometimes increasing and sometimes decreasing with frequency [50,54–57,60]. Inset in Fig. 3 shows the inelastic case with a zoom in the low stress region.

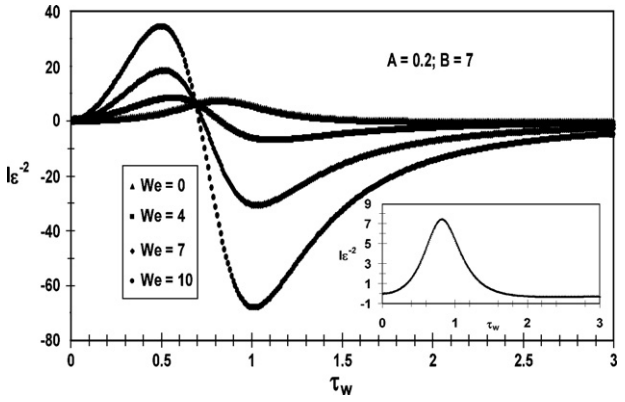


**Fig. 3.** Flow enhancement versus dimensionless wall stress as a function of the Weissenberg number ($We$): (i) 0, (ii) 4, (iii) 7; (iv) 10. Inset: inelastic liquid. The dimensionless numbers used in the simulation are: $A = 0.2$ and $B = 7$.

It should be noted that the existence of both lower and upper viscosity plateaus causes that at a given wall stress, a maximum ($I\varepsilon^{-2}$) occurs. The value of the maximum in $I$ (%) is directly related to the ratio of these viscosities, and same results can be obtained with different constitutive equations [50,54–57,60,71].

However, Phan-Thien, Manero and Walters [50,54–60] showed that the flow enhancement is always positive even if elasticity is included. In contrast, the BMP model predicts a region where the flow enhancement is negative due to the convexity of the flow curve. Similar behavior has been found in the White–Metzner model when a Carreau–Yasuda expression is used to represent the viscosity function as reported by Bird et al. [49].

Fig. 4 shows the zeroth-order flow curve for several values of the non-dimensional number $A$ (which accounts for the ratio of kinetics of rupture and structure time) at a fixed value of the non-dimensional number $B$. All curves are monotonically increasing functions of the shear rate. For low values of $A$ (<1) the curves show an extended constant viscosity region, whereas higher values of $A$ cause the extent of the Newtonian region to decrease. The slope of the shear thinning region is the same for all curves as can be seen in the inset of this figure.

In Fig. 5, the flow enhancement ($I\varepsilon^{-2}$) versus wall stress for different values of the parameter $A$ is shown. The other parameters employed in the simulation are $We = 10$ and $B = 7$. To analyze systematically the effect of the thixotropy, the value of the kinetic constant is changed to $k = G_0^{-1}$, enabling $A$ to be the ratio $A = \eta_0/G_0/\lambda$. When the value of $A$ lies in the range $0 \leq A < 1$, the structure does not recover during the deformation period and hence the resonance curves are dramatically shifted due to the evolution of the system structure. Nevertheless, the magnitude of the maxima and minima is the same for all curves. The shifting implies that for a thixotropic fluid, the system needs more energy to obtain the same flow enhancement. In contrast, when the value of $A$ lies in the range of $1 \leq A \leq 10$, the structure recovers quickly and the curves are shifted to lower wall stresses. It is important to note

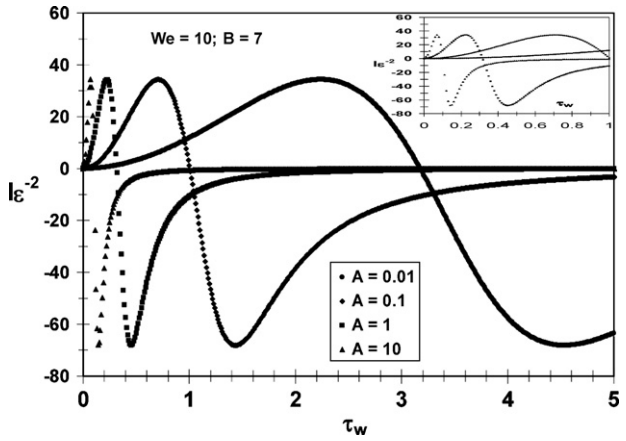


**Fig. 5.** Flow enhancement versus dimensionless wall stress for various values of the parameter A:(i) 0.01, (ii) 0.1, (iii) 1, and (iv) 10. Inset: Flow enhancement in the region of small wall stresses. $We = 10$ and $B = 7$.

**Table 1**
Values of the parameters used in the model as a function of CTAT concentration [33].

| $C_{CTAT}$ (wt.%) | $\eta_0^{-1}$ (Pa s)$^{-1}$ | $\eta_\infty^{-1}$ (Pa s)$^{-1}$ | $k \times 10^{-6}$ (Pa)$^{-1}$ | $\lambda$ (s) | $G_0$ (Pa) |
|---|---|---|---|---|---|
| 5 | 0.0275 | 19.8 | 250.0 | 0.12 | 41.5 |
| 10 | 0.0061 | 15.0 | 30.3 | 0.33 | 176.0 |
| 15 | 0.0050 | 12.6 | 10.5 | 0.38 | 380.0 |
| 20 | 0.0042 | 12.0 | 4.2 | 0.42 | 620.0 |

that Figs. 2, 3 and 5 show regions where the flow enhancement is a non-monotonically function of the wall stress. The maximum in the curves has been reported by several authors employing different constitutive equations. However, the minimum in the curves has not been reported experimentally and it is only reported in theoretical works. Constitutive equations that include a relaxation time that depends on the second invariant of the strain-rate tensor (e.g. White–Metzner, BMP and modify BMP models) predict this negative enhancement which is caused by the convexity of the constitutive curve [47,72,75]. Equations that contain second derivatives of the viscosity function and/or the shear stress (Eq. (25)), present negative enhancement due to the change in convexity of the flow curve (see Fig. 2). Nevertheless, an equation of lower order derivatives presents a similar behavior due to elastic effects associated to the material (Eq. (25)). In contrast, when elastic effects are negligible (see *We* number value in Tables 2 and 3), the negative region tends to disappear (see insets in Figs. 5 and 8). For these reasons, it is clear that the effect of the negative flow enhancement can be attributed to the mathematical properties of the constitutive equation and flow curve.

### 6.2. Predictions of the flow enhancement using worm-like solutions data

In Fig. 6, predictions of the flow enhancement ($I\varepsilon^{-2}$) versus wall stress using viscometric data of CTAT at different concentrations

**Table 2**
Values of the dimensionless numbers used in the model as a function of CTAT concentration. The parameters employed in the simulation are: $M = 1$; $\omega = 1.0$ rad/s; $a = 5 \times 10^{-2}$ m; $\rho = 1000$ kg/m$^3$.

| wt.% | Re | $\omega^*$ | *We* | *A* | *B* | $I_{Max}\varepsilon^{-2}$ | $\tau_w$ ($I_{Max}$) |
|---|---|---|---|---|---|---|---|
| 5 | 0.0690 | 0.12 | 0.876 | 0.0760 | 720 | 43.25 | 1.4 |
| 10 | 0.0153 | 0.33 | 0.931 | 0.0150 | 2459 | 7.44 | 5.2 |
| 15 | 0.0125 | 0.38 | 0.526 | 0.0055 | 2520 | 4.24 | 2.8 |
| 20 | 0.0105 | 0.42 | 0.384 | 0.0024 | 2857 | 4.45 | 12.2 |

$Re = \frac{\rho\omega a^2}{\eta_0}$; $\omega^* = \omega\lambda$; $We = \frac{\eta_0}{G_0}\omega$; $A = \frac{k\eta_0}{\lambda}$; $B = \frac{\eta_0}{\eta_\infty}$.

**Table 3**
Values of the dimensionless numbers used in the model for several frequencies. The values of the ratio of the pipe and the density of the complex liquid are: $M = 1$; $a = 5 \times 10^{-2}$ m; $\rho = 1000$ kg/m$^3$.

| 10 wt.% | $\beta$ | *A* | *B* | *De* | $I_{Max}\varepsilon^{-2}$ | $\tau_w$ ($I_{Max}$) |
|---|---|---|---|---|---|---|
| $\omega_1^* = 0.12$ | 0.573 | 0.076 | 720 | 7.30 | 10.82 | 1.4 |
| $\omega_2^* = 0.24$ | 0.573 | 0.076 | 720 | 7.30 | 43,25 | 1.4 |
| $\omega_3^* = 0.36$ | 0.573 | 0.076 | 720 | 7.30 | 97.20 | 1.4 |

$\beta = \frac{a^2/\lambda}{\eta_0/\rho}$; $De = \frac{\eta_0/G_0}{\lambda}$; $A = \frac{k\eta_0}{\lambda}$; $B = \frac{\eta_0}{\eta_\infty}$;
$\omega_1 = 1$ rad/s; $\omega_2 = 2$ rad/s; $\omega_3 = 3$ rad/s.

($T = 30\,^\circ$C), reported by Soltero et al. [76], are plotted. Parameters employed in the model as functions of CTAT concentration are given in Table 1 and the corresponding dimensionless groups are disclosed in Table 2.

For the solution with 5 wt.% CTAT (see inset) the flow enhancement increases and for $1.2 < \tau_w < 1.5$ a drastic enhancement is observed with a maximum in the resonance curve of $I\varepsilon^{-2} = 43.25$ at $\tau_w = 1.4$. In this region, the fluid experiences a pronounced shear-thinning behavior. The maximum flow enhancement is found for the 5 wt.% CTAT content, it has been reported by several authors that the shear thinning effect is responsible of the flow enhancement as reported in the literature [40–71].

Nevertheless, the 5 wt.% solution has the minimum shear thinning effect, related to the value of the dimensionless *B* number (see Table 2). Thixotropy was found to have a negative effect on the flow enhancement, thus the maximum concentration of CTAT shares the maximum thixotropy value (thixotropy is related to the dimensionless number *A*, see Table 2) and so the flow enhancement decreases due to high thixotropy. This is believed to be the cause of the maximum flow enhancement at the minimum CTAT content.

For a CTAT content of 10 wt.%, the maximum in the curve is $I\varepsilon^{-2} = 7.44$ at $\tau_w = 5.2$. For the 15 wt.% solution, the maximum in the curve is $I\varepsilon^{-2} = 4.24$ at $\tau_w = 2.8$, lower than that at 10 wt.%. Finally, for a CTAT content of 20 wt.%, the maximum in the curve is $I\varepsilon^{-2} = 4.45$ at $\tau_w = 12.2$. Despite that the solution is structured ($A = 0.0024$), this structure is destroyed by flow exhibited by the pronounced shear thinning. Furthermore, the maximum is shifted to larger wall stresses, implying a larger energy requirement for flow enhancement.

There is a characteristic wall stress for the maximum flow enhancement in the curves; this maximum is related to the structural changes that the fluid undergoes, as *B* is quite high in strong shear thinning fluids (see Table 2). The value of the maximum is determined by the coupling among the kinetic, viscous and structural properties of the BMP model. Furthermore, it is important to

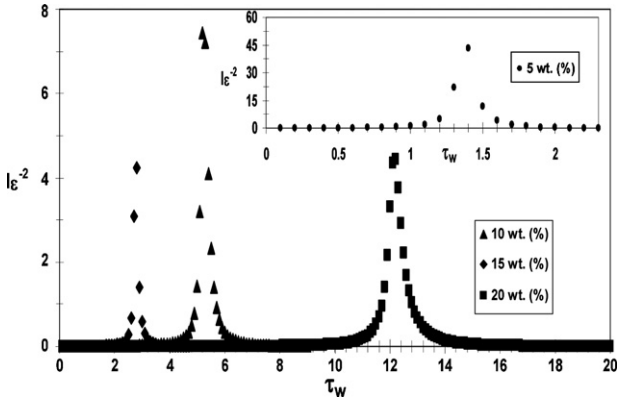


**Fig. 6.** Flow enhancement versus dimensionless wall stress for a 5 wt.% CTAT solution at $T = 30\,^\circ$C. In the inset, (i) 10 wt.%, (ii) 15 wt.%, (iii) 20 wt.%. Non-dimensional numbers used in the simulation are given in Table 2.

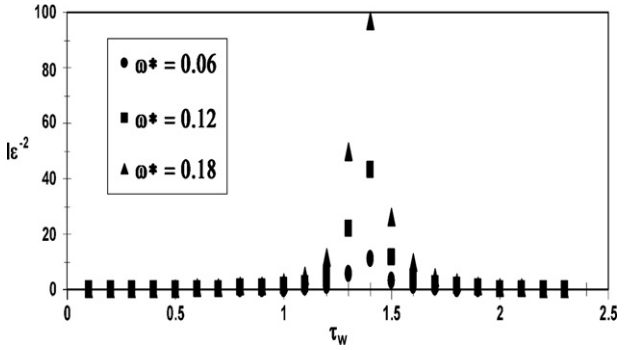


**Fig. 7.** Flow enhancement versus dimensionless wall stress for a 5 wt.% CTAT solution at $T = 30\,^{\circ}C$ as a function of the dimensionless frequency. Parameters employed in the simulation are given in Table 3.

**Table 4**
Values of the dimensionless numbers used in the model as a function of CTAT concentration. The parameters employed in the simulation are: $M = 1$; $a = 5 \times 10^{-2}$ m; $\rho = 1000\,kg/m^3$.

| wt.% | $\beta$ | $A$ | $B$ | $De$ | $\tau_w$ | $\omega^*_{crit}$ |
|---|---|---|---|---|---|---|
| 5 | 0.573 | 0.076 | 720 | 7.30 | 0.23 | 1.7 |
| 10 | 0.046 | 0.015 | 2459 | 2.82 | 0.23 | 21.5 |
| 15 | 0.033 | 0.0055 | 2520 | 1.39 | 0.23 | 30 |
| 20 | 0.025 | 0.0024 | 2857 | 0.914 | 0.23 | 40 |

$\beta = \frac{a^2/\lambda}{\eta_0/\rho}$; $De = \frac{\eta_0/G_0}{\lambda}$; $A = \frac{k\eta_0}{\lambda}$; $B = \frac{\eta_0}{\eta_\infty}$.

note that negative flow enhancement is very small and cannot be observed due to the scale of the figure. This small negative value is associated to small *We* as determined experimentally, since negative flow enhancement is evident to disappear for very small values of the Weissenberg number (see Fig. 3).

In Fig. 7, the flow enhancement ($I\varepsilon^{-2}$) versus wall stress for a 5 wt.% solution with varying frequency is shown. To quantify the flow enhancement dependence on the frequency, the following ratios are calculated: $I_{\omega^*=0.12}/I_{\omega^*=0.06} = 43.25/10.82 \cong 2^2$ and $I_{\omega^*=0.18}/I_{\omega^*=0.06} = 97.20/10.82 \cong 3^2$. The frequency dependence of the maxima is clearly depicted, contrasting with other results that predict that the flow enhancement is a decreasing function of frequency [41,47,57]. A relationship between the non-dimensional frequency and the flow enhancement follows the form suggested in (31), namely, $I_1/I_0 \cong (\omega_1^*/\omega_0^*)^2$, where $I_0$ is the flow enhancement calculated at the dimensional frequency $\omega_0^*$ and $\omega_1^* = N^2\omega_0^*$ is a factor of $\omega_0^*$ ($N \in R^+$).

In Fig. 8, the flow enhancement ($I\varepsilon^{-2}$) versus frequency for various CTAT solutions is larger in the more dilute solutions. The flow

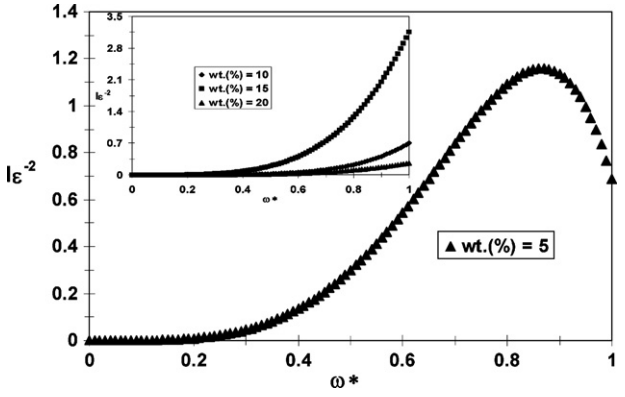


**Fig. 8.** Flow enhancement versus dimensionless frequency for a 5 wt.% CTAT solution at $T = 30\,^{\circ}C$ ($\tau_w = 0.23$). In the inset (i) 10 wt.%, (ii) 15 wt.%, and (iii) 20 wt.%. Dimensionless numbers used in the simulation are given in Table 3.

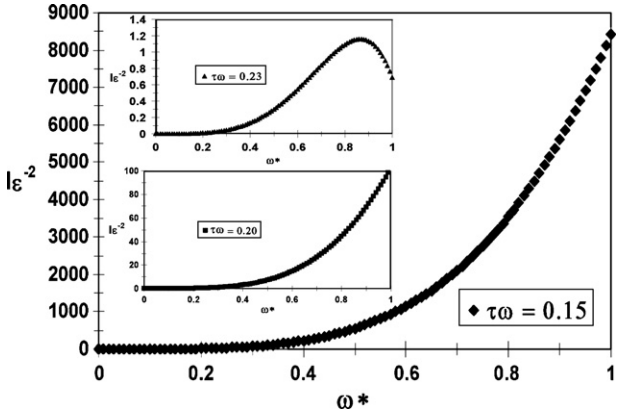


**Fig. 9.** Flow enhancement versus dimensionless frequency for a 5 wt.% CTAT solution at $T = 30\,^{\circ}C$ ($\tau_w = 0.15$). In the insets $\tau_w$ = (i) 0.20, (ii) 0.23. Parameters used in the simulation are given in Table 4.

enhancement is predicted to increase with frequency up to a maximum and thereafter it decreases.

Likewise, Fig. 9 shows the flow enhancement ($I\varepsilon^{-2}$) versus non-dimensional frequency for a 5 wt.% solution and for various wall stresses. It is clear that the flow enhancement is an increasing function of the wall stress and frequency, but in all cases a maximum is predicted.

## 7. Conclusions

In this work, a perturbation solution to a pulsating pressure gradient flow of a complex liquid using the BMP model is presented for a general class of pressure gradient noises. The structural liquid was characterized by the BMP equation which couples a time-dependent equation for the structure changes with the upper-convected Maxwell constitutive equation. The evolution equation for the structural changes was conceived to account for the kinetic process of breakage and reformation of the micelles under flow.

The following conclusions are highlighted:

- The flow enhancement and power requirement for the BMP model (Eqs. (25) and (27) can be separated into two contributions, inelastic and elastic and is a function of the amplitude of the oscillations, perturbation parameter and *We* (all squared), and the dimensionless numbers $A$ and $B$ (representing viscoelastic, kinetic and structural effects).
- A necessary condition to obtain a positive flow enhancement in a structural liquid is that the fluid experiments undergoes transition from a high structured state to a less structured one induced by flow, i.e. $B = \eta_0\eta_\infty^{-1} \gg 1$.
- The viscoelastic, kinetic and structural mechanisms in the BMP model were characterized by associating non-dimensional numbers to each mechanism: (i) $A = \frac{k\eta_0}{\lambda}$, (ii) $B = \eta_0\eta_\infty^{-1}$ and (iii) $We = \omega\eta_0 G_0^{-1}$. The first one is associated to the kinetic, viscous, and structural process and the second one to the level of the structure in the liquid. The third group is the pulsating Weissenberg number which is a measure of the system viscoelasticity.
- In a complex liquid, thixotropy can be interpreted as a particular case of the rupture and structural mechanisms in the system, i.e. $De = \lambda_0\lambda^{-1} \subset A = k\eta_0\lambda^{-1}$, when the kinetic constant is identified as a normalized constant for the shear stress, i.e. $k = G_0^{-1}$.
- The flow enhancement is a function of the concentration of the solution, in this case CTAT. In most cases, the flow enhancement decreases when the concentration of the solution increases,

because the structural process dominates over the viscoelastic contribution and this is related to thixotropy.

- Qualitatively, the flow enhancement for CTAT solution increases with the non-dimensional frequency according to $I_1 \cong (\omega_1^*/\omega_0^*)^2 I_0$ (when the elastic effects are neglected). On the other hand, when the elastic force dominates, the flow enhancement follows the relationship $I_1 \cong (\omega_1^*/\omega_0^*)^4 I_0$, where $I_0$, $I_1$ are the flow enhancements calculated at frequency $\omega_0^*$ and $\omega_1^* = N\omega_0^*$ ($N \in R^+$).

## 8. Future work

- It would be worthwhile to compare the theoretical predictions of the effect of thixotropy with experimental observations. For example, by using viscoelastic surfactants such as CTAT, EHAC, liquid crystalline suspensions or associative polymers.
- One of the most interest effects of complex fluids is the shear-banding flow, where due to mechanical and thermodynamic instabilities the system separates in regions of different viscosities. The drastic shear-thinning behavior may produce a very high enhancement in the context of pulsating flows.
- Analysis on the effect of longitudinal and transversal oscillating flow on the viscous dissipation and inertial effects in polymer extrusion.

## Acknowledgements

The authors wish to acknowledge the support of the National Council of Science and Technology of Mexico (CONACYT) Projects 162980 and 100195.

## References

[1] Y.C. Fung, Biomechanics, second ed., Springer, New York, 1997.
[2] M. Zamir, The Physics of Pulsatile Flow, Springer-Verlag, New York, 2000.
[3] J.K.J. Li, Dynamics of the Vacular System, World Scientific, Singapore, 2004.
[4] M.A. Moyers-Gonzalez, R.G. Owens, J. Fang, On the high frequency oscillatory tube flow of healthy human blood, J. Non-Newton. Fluid Mech., 2009. doi:10.1016/j.jnmfm.2009.06.005.
[5] M.A. Moyers-Gonzalez, R.G. Owens, J. Fang, A non-homogeneous constitutive model for human blood. Part I. Model derivation and steady flow, J. Fluid Mech. 617 (2008) 327–354.
[6] M.A. Moyers-Gonzalez, R.G. Owens, A non-homogeneous constitutive model for human blood. Part II. Asymptotic solution for large Péclet numbers, J. Non-Newton. Fluid Mech. 155 (2008) 146–160.
[7] M.A. Moyers-Gonzalez, R.G. Owens, A non-homogeneous constitutive model for human blood. Part III. Oscillatory flow, J. Non-Newton. Fluid Mech. 155 (2008) 161–173.
[8] D.S. Sankar, K. Hemalatha, Pulsatile flow of Herschel–Bulkley fluid through catherized arteries—a mathematical model, Appl. Math. Model 31 (2007) 1497–1517.
[9] J. Fang, R.G. Owens, Numerical simulations of pulsatile blood flow using a new constitutive model, Biorheology 43 (2006) 637–660.
[10] M. El-Shahed, Pulsatile flow of blood through a stenosed porous medium under periodic body acceleration, Appl. Math. Comput. 138 (2003) 479–488.
[11] G. de Luca, A.D. Rey, Dynamics interactions between nematic point defects in the extrusion duct of spiders, J. Chem. Phys. 124 (2006) 14904/1–14904/8.
[12] L.R.P. De Andrade Lima, A.D. Rey, Pulsatile flows of Leslie–Ericksen liquid crystals, J. Non-Newton. Fluid Mech. 135 (2006) 32–45.
[13] L.R.P. De Andrade Lima, A.D. Rey, Pulsatile Poiseuille flow of discotic mesophases, Chem. Eng. Sci. 60 (2005) 6622–6636.
[14] J. Casulli, J.R. Clermont, A. Von Ziegler, B. Mena, The oscillating die: a useful concept in polymer extrusion, J. Polym. Eng. Sci. 30 (1990) 1551–1556.
[15] A.I. Isayev, C.M. Wong, X. Zeng, Flow of thermoplastic in annular die under orthogonal oscillations, J. Non-Newton. Fluid Mech. 34 (1990) 375–397.
[16] C.M. Wong, C.H. Chen, A.I. Isayaev, Flow of thermoplastic in an annular die under parallel oscillations, Polym. Eng. Sci. 30 (1990) 1574–1584.
[17] J. Dunwoody, The effects of inertia and infinite amplitude on oscillatory plane shear flow of K-BKZ fluids such as LPDE melts, J. Non-Newton. Fluid Mech. 65 (1996) 195–200.
[18] F. Ding, Giacomin, R.B. Bird, C.B. Kweon, Viscous dissipation with fluid inertia in oscillatory shear flow, J. Non-Newton. Fluid Mech. 86 (1999) 359–374.
[19] J.R. Herrera-Velarde, B. Mena, A note on Newtonian and non-Newtonian oscillatory pipe flow, Rev. Mexicana Física 46 (6) (2000) 566–571.
[20] J.R. Herrera-Velarde, B. Mena, Viscous dissipation of a power law fluid in a oscillatory pipe flow, Rev. Mexicana Física 47 (4) (2001) 351–356.
[21] J.R. Herrera Velarde, R. Zenit, B. Mena, Measurement of the temperature rise in non-Newtonian oscillatory pipe flows, J. Non-Newton. Fluid Mech. 109 (2003) 157–176.
[22] J. Edward Glass, A perspective on the history of a current research in surfactant-modified, water-soluble polymers, J. Coat. Technol. 73 (913) (2001) 79–98.
[23] B Olayiwola, P. Wazel, Cross flow transport and heat transfer enhancement in laminar pulsed flow, Chem. Eng. Process. J. 47 (2008) 929–937.
[24] E. Maucci, R.J. Martinuzzi, Cedric L. Briens, G. Wild, Modelling of transient mass transfer in liquid and liquid–solid pulsating systems: applications and extension to heat transfer, Can. J. Chem. Eng. 79 (2001) 329–340.
[25] A.B.D. Brown, A.R. Rennie, Images of shear-induced phase separation in a dispersion of hard nanoscale discs, Chem. Eng. Sci. 56 (2001) 2999–3004.
[26] G.H. Brown, J.J. Wolken, Liquid Crystals and Biological Structures, Academic Press, New York, 1979.
[27] A.D. Rey, Theory of linear viscoelasticity of cholesteric liquid crystals, J. Rheol. 44 (4) (2000) 855–869.
[28] A.D. Rey, M.M. Deen, Dynamical phenomena in liquid-crystalline materials, Annu. Rev. Fluid Mech. 34 (2002) 233–266.
[29] L.R.P. de Andadre Lima, A.D. Rey, Poiseuille flow of Leslie Ericksen discotic liquid crystals: solution multiplicity, multistability, and non-Newtonian rheology, J. Non-Newton. Fluid Mech. 110 (2–3) (2003) 103–142.
[30] L.R.P. de Andrade Lima, A.D. Rey, Linear and nonlinear viscoelasticity of discotic nematics under transient Poisuille flows, J. Rheol. 47 (5) (2003) 1261–1282.
[31] L.R.P. de Andrade Lima, A.D. Rey, Linear viscoelasticity of discotic mesophases, Chem. Eng. Sci. 59 (2004) 3891–3905.
[32] Jiang Yang, Viscoelastic wormlike micelles and their applications, Colloid Interface Sci. 7 (2002) 276–281.
[33] M.E. Cates, Reptation of living polymers: dynamics of entangled polymers in the presence of reversible chain-scission reactions, Macromolecules 20 (1987) 2289–2296.
[34] M.E. Cates, S.J. Candau, Statics and dynamics of worm-like surfactants micelles, J. Phys. Condens. Matter 2 (1990) 6869–6892.
[35] N.A. Spenley, M.E. Cates, T.C.B. McLeish, Non-linear rheology of wormlike micelles, Phys. Rev. Lett. 71 (1993) 939–942.
[36] N.A. Spenley, M.E. Cates, Pipe models for entangled fluids under strong shear, Macromolecules 27 (1994) 3850–3858.
[37] N.A. Spenley, X.F. Yuan, M.E. Cates, Non-monotonic constitutive laws and the formation of shear banded flows, J. Phys. II France 6 (1996) 551–571.
[38] J.-F. Berret, Transient rheology of wormlike micelles, Langmuir 13 (1997) 2227–2234.
[39] A.G. Fredrickson, Principles and Applications of Rheology, Prentice-Hall, Englewood Cliffs, 1964.
[40] H.A. Barnes, P. Townsend, K. Walters, Flow of non-Newtonian liquids under varying pressure gradient, Nature 224 (1969), 85-58.
[41] H.A. Barnes, P. Townsend, K. Walters, On pulsatile flow of non-Newtonian liquids, Rheol. Acta 10 (1971) 517–527.
[42] A. Gianneto, G. Baldi, Flusso laminar pulsate di fluidi non newtonian, Quaderni dell Ingegnere Chim. Italiano 6 (11) (1970) 186–197.
[43] M.F. Edwards, D.A. Nellist, W.L. Wilkinson, Unsteady laminar flows of non-Newtonian fluid in pipes, Chem. Eng. Sci. 27 (1972) 295–306.
[44] M.F. Edwards, D.A. Nellist, W.L. Wilkinson, Pulsating flows of non-Newtonian fluids in pipes, Chem. Eng. Sci. 27 (1972) 545–553.
[45] M.F. Edwards, D.A. Nellist, W.L. Wilkinson, Laminar pulsed flow non-Newtonian fluids, Chem. Eng. Sci. 28 (2) (1972) 671–672.
[46] D.W. Sundstrom, A. Kaufman, Pulsating flow of polymeric solutions, Ind. Eng. Chem. Process. Des. Dev. 16 (3) (1977) 320–325.
[47] R.B. Bird, R.C. Armstrong, O. Hassager, Dynamics of Polymeric Liquids, John Wiley & Sons, New York, 1977.
[48] O. Manero, B. Mena, An interesting effect in non-Newtonian flow in oscillating pipes, Rheol. Acta 19 (1977) 277–284.
[49] J.M. Davies, S. Bhumiratana, R.B. Bird, Elastic and inertial effects in pulsatile flow of polymeric liquids in circular tubes, J. Non-Newton. Fluid Mech. 3 (1978) 237–259.
[50] N. Phan-Thien, On pulsating flow of polymeric fluids, J. Non-Newton. Fluid Mech. 4 (1978) 167–176.
[51] J.Y. Kazakia, R.S. Rivlin, The influence of vibration on Poiseuille flow of non-Newtonian fluids, I, Rheol. Acta 18 (1978) 210–226.
[52] J.Y. Kazakia, R.S. Rivlin, The influence of vibration on Poiseuille flow of non-Newtonian fluids II, Rheol. Acta 18 (1979) 244–255.
[53] B. Mena, O. Manero, D.M. Binding, Complex flow of viscoelastic fluids through oscillating pipes, interesting effects and applications, J. Non-Newton. Fluid Mech. 5 (1979) 427–448.
[54] N. Phan-Thien, Flow enhancement mechanism of a pulsating flow of non-Newtonian liquids, Rheol. Acta 19 (1980) 285–290.
[55] N. Phan-Thien, The effects of longitudinal vibration on pipe flow of a non-Newtonian fluid, Rheol. Acta 19 (1980) 539–547.
[56] O. Manero, K. Walters, On elastic effects in unsteady pipe flows, Rheol. Acta 19 (1980) 277–284.
[57] N. Phan-Thien, On pulsating flow of a polymer fluids: strain-dependent memory kernels, J. Rheol. 25 (3) (1981) 293–314.
[58] N. Phan-Thien, On a pulsating flow of slightly non-Newtonian liquids, J. Mécanique Théorique Appliqué 1 (1982) 81–89.
[59] N. Phan-Thien, J. Dudek, Pulsating flow of a plastic fluid, Nature 296 (1982) 843–844.
[60] N. Phan-Thien, J. Dudek, Pulsating flow revisited, J. Non-Newton. Fluid Mech. 11 (1982) 147–161.

[61] T. Kajiuchi, A. Saito, Flow enhancement of laminar pulsating flow of Bingham plastic fluids, J. Chem. Eng. Jpn. 17 (1) (1984) 34–38.
[62] N. Mori, K. Wakabayashi, A. Horikawa, K. Nakamura, Measurements of pulsating and oscillating flows on non-Newtonian fluids through concentric and eccentric cylinders, Rheol. Acta 23 (1984) 508–513.
[63] E.M. Khabakhpasheva, V.I. Popov, A.N. Kekalov, E.S. Mikhailova, Pulsating flow of a viscoelastic fluids in tubes, J. Non-Newton. Fluid Mech. 33 (1989) 289–304.
[64] A. Siginer, A. Valenzuela Rendon, Energy consideration in the flow enhancement of viscoelastic liquids, Trans. ASME—J. Appl. Math. 60 (1993) 344–351.
[65] P. Towsend, Numerical solutions of some unsteady flows of elastico-viscous liquid, Rheol. Acta 12 (1973) 13–18.
[66] K.J. Hammad, G.C. Vradis, Viscous dissipation and heat transfer in pulsatile flows of a yield stress fluid, Int. Commun. Heat Mass Transf. 23 (5) (1996) 599–612.
[67] J.R. Herrera-Velarde, B. Mena, A note on Newtonian and non-Newtonian oscillatory pipe flow, Rev. Mexicana de Física 46 (6) (2000) 566–571.
[68] L.R.P. de Andrade Lima, A.D. Rey, Pulsatile flow of discotic mesophases, Chem. Eng. Sci. 60 (2005) 6622–6636.
[69] L.R.P. de Andrade Lima, A.D. Rey, Pulsatile flows of Leslie–Ericksen liquid crystals, J. Non-Newton. Fluid Mech. 133 (2006) 32–45.
[70] L.R.P. de Andrade Lima, A.D. Rey, Back-flow in pulsatile flows of Leslie Ericksen liquid crystals, Liquid Crystals 33 (6) (2006) 711–712.
[71] E.E. Herrera, F. Calderas, A.E. Chávez, O. Manero, B. Mena, Effect of random longitudinal vibrations pipe on the Poiseuille flow of a complex liquid, Rheol. Acta 48 (2009) 779–800.
[72] F. Bautista, J.M. De Santos, J.E. Puig, O. Manero, Understanding thixotropic and antithixotropic behavior of viscoelastic micellar solutions and liquid crystalline dispersions. The model, J. Non-Newton. Fluid Mech. 80 (1999) 93–113.
[73] F. Bautista, J.F.A. Soltero, J.H. Pérez–López, J.E. Puig, O. Manero, On the shear banding flow of elongated micellar solutions, J. Non-Newton. Fluid Mech. 94 (2000) 57–66.
[74] F. Bautista, J.F.A. Soltero, E.R. Macias, O. Manero, On the shear banding flow of wormlike micelles, J. Phys. Chem. B 106 (2002) 13018–13026.
[75] O. Manero, F. Bautista, J.F.A. Soltero, J.E. Puig, Dynamics of worm-like micelles: the Cox-Merz rule, J. Non-Newton. Fluid Mech. 106 (2002) 1–15.
[76] J.F.A. Soltero, J.E. Puig, O. Manero, Rheology of cetyltrimethylammonium p-toluenesulfonate-water system. 3. Nonlinear viscoelasticity, Langmuir 15 (1999) 1604–1612.
[77] F. Calderas, A. Sánchez-Solis, A. Maciel, O. Manero, The transient flow of the PETPEN-montmorillonite clay nanocomposite. Macromol. Symp. (283–284) (2009) 354–360. doi:10.1002/masy.200950942.
[78] A.J. Mendoza-Fuentes, R. Montiel, R. Zenit, O. Manero, On the flow of associative polymers past a sphere: evaluation of negative wake criteria, Phys. Fluids 21 (2009), 033104/1-13.
[79] A. Acierno, F.P. La Mantia, G. Marrucci, G. Titomanlio, A non linear viscoelastic model with structure dependent relaxation times. I. Basic formulation, J. Non-Newton. Fluid Mech. 1 (1976) 125–146.
[80] H. Giesekus, Die Elastizitat von Flussigkeiten, Rheol. Acta 5 (1966) 29–35.
[81] H. Giesekus, A simple constitutive equation for polymer fluids based on the concept of deformation-dependent tensorial mobility, J. Non-Newton. Fluid Mech. 11 (1982) 69–109.
[82] H. Giesekus, On configuration-dependent generalized Oldroyd derivatives, J. Non-Newton. Fluid Mech. 14 (1984) 47–65.
[83] H. Giesekus, Constitutive equation for polymer fluids based on the concept of configuration dependent molecular mobility: a generalized mean-configuration model, J. Non-Newton. Fluid Mech. 17 (1985) 349–372.
[84] D. De Kee, C.F. Chan Man Fong, Rheological properties of structured fluids, Polym. Eng. Sci. 34 (1994) 438–445.
[85] E.E. Herrera, Flujo oscilante de líquidos complejos, Ph.D. thesis, División de Estudios de Posgrado de la Facultad de Química, Universidad Nacional Autónoma de México, (2009).
[86] A.M. Yaglom, in: R.A. Silverman (Ed.), An Introduction to the Theory of Stationary Random Functions Translated, Prentice-Hall, Englewood Cliffs, NJ, 1965.